

NAVAL POSTGRADUATE SCHOOL

Monterey, California



THESIS

ACOUSTIC ROOM DE-REVERBERATION USING TIME-REVERSAL ACOUSTICS

by

David W. Liddy
John F. Holmes

September 1999

Thesis Advisor:
Co-Advisor:

Andrés Larraza
Bruce Denardo

Approved for public release; distribution is unlimited.

REPORT DOCUMENTATION PAGE			Form Approved OMB No. 0704-0188	
Public reporting burden for this collection of information is estimated to average 1 hour per response, including the time for reviewing instruction, searching existing data sources, gathering and maintaining the data needed, and completing and reviewing the collection of information. Send comments regarding this burden estimate or any other aspect of this collection of information, including suggestions for reducing this burden, to Washington Headquarters Services, Directorate for Information Operations and Reports, 1215 Jefferson Davis Highway, Suite 1204, Arlington, VA 22202-4302, and to the Office of Management and Budget, Paperwork Reduction Project (0704-0188) Washington DC 20503.				
1. AGENCY USE ONLY	2. REPORT DATE September 1999	3. REPORT TYPE AND DATES COVERED Master's Thesis		
4. TITLE AND SUBTITLE Acoustic Room De-reverberation Using Time-Reversal Acoustics		5. FUNDING NUMBERS		
6. AUTHORS Liddy, David W., Holmes, John F.				
7. PERFORMING ORGANIZATION NAME(S) AND ADDRESS(ES) Naval Postgraduate School Monterey CA 93943-5000		8. PERFORMING ORGANIZATION REPORT NUMBER		
9. SPONSORING/MONITORING AGENCY NAME(S) AND ADDRESS(ES)		10. SPONSORING/MONITORING AGENCY REPORT NUMBER		
11. SUPPLEMENTARY NOTES The views expressed in this thesis are those of the authors and do not reflect the official policy or position of the Department of Defense or the U.S. Government.				
12a. DISTRIBUTION/AVAILABILITY STATEMENT Approved for public release; distribution is unlimited.			12b. DISTRIBUTION CODE	
13. ABSTRACT (maximum 200 words) This thesis probes the performance of one-channel time-reversal acoustics in a chamber in terms of the geometry of the cavity. In particular, a rectangular chamber is compared to an enclosure that has a stadium shape. The mode structure in the rectangular cavity is highly symmetric, while it is highly irregular in the stadium-shaped cavity. Time-reversal acoustic techniques produce an improved focus in the latter. The focusing quality is determined as a function of frequency, time-reversal window size, and spatial extent. A scheme for encrypted acoustic communication, both in air and underwater, that uses multiple broadband signals with identical bandwidth, Hanning window source spectra, and center frequencies separated by half the bandwidth, allowing for null detection between adjacent signals, is successfully investigated.				
14. SUBJECT TERMS: Time-Reversal Acoustics, Acoustic Communications, Acoustic Signal Processing, Reverberation, De-Reverberation			15. NUMBER OF PAGES 63	
			16. PRICE CODE	
17. SECURITY CLASSIFICATION OF REPORT Unclassified	18. SECURITY CLASSIFICATION OF THIS PAGE Unclassified	19. SECURITY CLASSIFICATION OF ABSTRACT Unclassified	20. LIMITATION OF ABSTRACT UL	

Approved for public release; distribution is unlimited.

ACOUSTIC ROOM DE-REVERBERATION USING TIME-REVERSAL ACOUSTICS

David W. Liddy
Lieutenant, United States Navy
B.S., University of South Carolina, 1993

John F. Holmes
Lieutenant Commander, United States Navy
B.S., University of Rochester, 1985

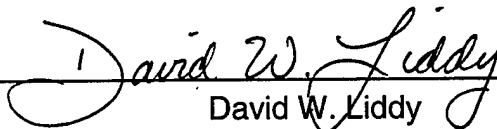
Submitted in partial fulfillment of the
requirements for the degree of

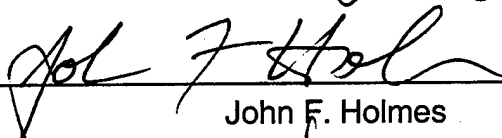
MASTER OF SCIENCE IN APPLIED PHYSICS

from the

**NAVAL POSTGRADUATE SCHOOL
September 1999**

Authors:


David W. Liddy


John F. Holmes

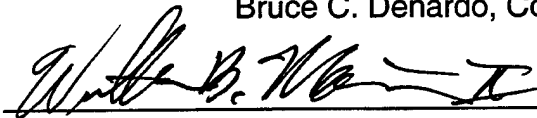
Approved by:



Andrés Larraza, Thesis Advisor



Bruce C. Denardo, Co-Advisor



William B. Maier, Chair, Department of Physics

ABSTRACT

This thesis probes the performance of one-channel time-reversal acoustics in a chamber in terms of the geometry of the cavity. In particular, a rectangular chamber is compared to an enclosure that has a stadium shape. The mode structure in the rectangular cavity is highly symmetric, while it is highly irregular in the stadium-shaped cavity. Time-reversal acoustic techniques produce an improved focus in the latter. The focusing quality is determined as a function of frequency, time-reversal window size, and spatial extent. A scheme for encrypted acoustic communication, both in air and underwater, that uses multiple broadband signals with identical bandwidth, Hanning window source spectra, and center frequencies separated by half the bandwidth, allowing for null detection between adjacent signals, is successfully investigated.

TABLE OF CONTENTS

I. INTRODUCTION	1
II. ACOUSTIC MODES IN AN ENCLOSURE	5
A. RESONANT MODES IN A RECTANGULAR CAVITY	5
B. DISTRIBUTION OF FREQUENCY SPACINGS.....	7
III. APPARATUS	11
A. ACOUSTIC CAVITY	11
B. ACOUSTIC DRIVER.....	12
C. MICROPHONE	13
IV. SPECTRAL AND MODE MEASUREMENTS OF THE CAVITIES	15
A. SPECTRUM MEASUREMENT	15
1. Rectangular Cavity.....	16
2. Stadium Cavity	18
B. FREQUENCY SPACING	19
C. NODAL MAPPING.....	22
1. Rectangular Cavity.....	22
2. Stadium Geometry	25
V. TIME-REVERSAL ACOUSTICS.....	27
A. OVERVIEW	27
1. Signal Processing Technique.....	29
2. Sound Propagation	30
B. ANALYSIS	32
1. TRA Focusing Quality as a Function of Frequency.....	32
2. TRA Focusing Quality as a Function of Window Size	33
3. Extent of Spatial Focusing	37
4. A Non-coherent Communication Scheme.....	39
VI. CONCLUSIONS AND FUTURE WORK.....	43
A. CONCLUSIONS	43
B. FUTURE WORK.....	44
APPENDIX. SPECTRAL AND MODE MEASUREMENT DATA	47
LIST OF REFERENCES.....	49
INITIAL DISTRIBUTION LIST.....	51

ACKNOWLEDGEMENTS

I wish to give recognition to:

My wife and family. Laurie, for her love and support throughout our marriage, especially during my studies at the Naval Postgraduate School and my fellowship with the CNO Strategic Studies Group (SSG) in Newport, RI. My eldest son, Greg, for helping us with his siblings and the household, and for filling in for me while I was away with the SSG. My entire family for their patience and understanding throughout my service to the Navy.

NPS Faculty. My thesis advisor, Professors Andrés Larraza, for his dedication and support throughout the past eighteen months. About one weekend per month for the 8 months that I was in Newport, I would return home to visit my family and to continue working on the experiment. Professor Larraza was always very accommodating throughout this process, meeting with me whenever it was convenient for my schedule. I am very fortunate he was so helpful, because I certainly could not have completed this thesis without him! I greatly appreciate the insightful, patient, and understanding manner with which he advised me and am very happy I had the opportunity to work with him.

Professors Bruce Denardo, and Tom Hofler for their time and dedication throughout this process. It was great to have the privilege to work with you.

Fellow Officers. My friend and co-author, John Holmes, for providing a valuable contribution to this thesis, working very hard in a very hectic time, and tolerating me as a roommate during our stay in Newport. My friends and TRA accomplices, Mike Heinemen and Mitch Shipley. Mike, for developing and helping me modify his excellent TRA software that made this project much less difficult; Mitch, for helping me get started with the Gagescope equipment.

NPS Staff. The entire Department of Physics technical support team whose efforts were instrumental to the success of this project.

THANK YOU!

David W. Liddy

I wish to give recognition to:

My wife Katie for her love and putting up with my lengthy time spent away from home while doing this research and participating in the CNO Strategic Studies Group. You made it possible for me to get through all of this with a smile on my face. I look forward to being with you everyday on the island of Guam (where America's Day begins). I love you very much.

My thesis advisors, Professors Andrés Larraza and Bruce Denardo, for their time and efforts in taking me on as a thesis student, and for their guidance throughout this process.

My cohort David Liddy, for tolerating me as a roommate during our time in Newport, and for taking me on as part of this thesis so late in the game. Good luck in your future endeavors. I know you will be successful. Until we see one another again in this small Navy of ours. As someone near and dear to us once said, "Never underestimate what I bring to this thesis."

My golfing support group: Jeff Bennett, Scott Bewley, and Ty Britt - keep it in the short grass and may you never get the yips.

The academic support group that assisted me in completing the course work: Pat Hall, D.J. Haynie, Pierre Hilaire, Paul Herbert and the rest of WC71.

David Grooms and George Jaksha, members of the physics technical support team here at the Naval Postgraduate School, whose efforts were instrumental in helping build the apparatus and gather the necessary equipment for this project.

THANK YOU!

John F. Holmes

I. INTRODUCTION

When you and a friend walk into an empty room with rigid walls, ceiling, and floor, the click-clack of your hard-sole shoes echoes throughout the room. Now, imagine placing yourselves far apart within the room. Because of the reverberation in such a room, maintaining a conversation between the two of you becomes very difficult. The reverberation is due to multiple reflections of sound at the surfaces of the room all arriving at different times. As a consequence, the intended receiver hears multiple arrivals due to the different propagation times of each individual path.

Similarly, for underwater acoustic propagation in shallow water environments, a narrow-band pulse generated by a point-like source spreads because of multi-path propagation due to reflections at the surface and at the bottom of the ocean or refractions within the interior. Each propagation path takes a different time, so that the transmitted pulse gives rise to multiple copies, not equally spaced in time, arriving at a receiver. The strong signal degradation due to the multipath propagation is further enhanced by high spatial and temporal variability of the channel conditions that exist in a typical underwater acoustic channel in shallow water environments.

In a communication link, the signal degradation due to multipath spreading causes Inter Symbol Interference (ISI) which is the interference between symbols due to multiple arrivals of each transmitted symbol. For example, in a shallow water channel a multipath spread of 100 ms with 1000 symbols per second, the

ISI extends to over 100 symbols. Also, as long propagation times decrease data throughput, available bandwidth is severely limited by transmission loss, which increases both in frequency and in range.

A novel technique called Time-Reversal Acoustics (TRA) can environmentally adapt the acoustic propagation effects of a complex medium in order to focus energy at a particular target range and depth. Additionally, estimates show that TRA focusing can be done at useful ranges (30 km) and over reasonable time scales (30 min) without updating the time-reversed signal under certain conditions (Kuperman et al). The TRA technique consists of digitizing the analog signal received by, say, a microphone or a hydrophone, time reversing it, and retransmitting it from a co-located source. If a wide-aperture array of receivers/transmitters is used, the time-reversed signal back at the point-like source is focused in time and space. For a small-aperture array, while the time-reverse signal back at the point-like source does not focus well in space, it still exhibits near-optimal focusing in time.

Using TRA, the multipath structure is eliminated because all of the propagation paths add coherently at the source location, which results in a reduced ISI of the communication link. Furthermore, due to spatial and temporal focusing there is a strong enhancement of the field at the focus location, which allows us to increase bandwidth and the transmission range.

Another exciting application for the TRA technique is called acoustic room de-reverberation where the apparent reverberation of a room is reduced by the ability to focus in space and time a full message. Surprisingly, in this case not an

array of elements, but a single element is required. Thus, a one-point time reversal in a cavity produces better results than a wide aperture time-reversal array in an open system.

Due to reciprocity, as long as the original source/receiver points are the only ones used in the operation, the time-reverse transmission and subsequent reception can be performed, undistinguishable by either point. In fact, for this experiment, the source and receiver remained in their original positions during the time-reversal transmission.

An important step toward useful naval and commercial applications of TRA is to fully explore the capabilities and limits. This exploration, often repetitive in nature, is most cost effectively done in tank-scale experiments and small rooms, and supplemented with numerical simulations.

In numerical investigations, Abrantes et al. (1999), Abrantes (1999), probed a scheme for an efficient, long-range, high-speed digital acoustic modem. It consists of transmitting multiple pulses with different center frequencies where the distance between neighboring center frequencies equals one-half the bandwidth of the pulse. This guarantees full resolution of a null between the two signals where the center frequencies are the next-nearest neighbors of each other. After initial transmission of the pulses, the TRA system "learns" the ocean transfer function. Subsequent transmissions can be made with overlapping signals, emulating multi-bit signals within a single reception. Thus for a full transmission bandwidth of 1 kHz and a pulse bandwidth of 200 Hz, this scheme can provide a rate of 2,000 bits/s. This is comparable to current rates with the

added benefits of longer range due to energy focusing and covert coding due to the inherent scrambling induced by the environment at points other than the intended receiver.

In this thesis we report room de-reverberation experiments performed in a rectangular cavity and a cavity shaped like a stadium. We have been able to produce a clear acoustic message transmitted from one point of the room to the another. The spatial extent of the focus is a half wavelength of sound indicating that the TRA possesses natural encryption for points other than the intended target. We have also performed the first experimental realization of Abrantes et al (1999) communication scheme.

The organization of this thesis is as follows. In Chapter II, we describe the theory for modes in a rectangular room and its distribution of eigenfrequency spacing. In contrast, we discuss the distribution of frequency spacing of an irregular geometry in the shape of a stadium. Chapter III deals with the description of the apparatus. Chapter IV provides the results of measurements of modes in both the rectangular and the stadium cavity and the distribution of measured frequencies of the rooms. Chapter V presents the results of different TRA measurements. Chapter VI provides conclusions and suggestions for future work.

II. ACOUSTIC MODES IN AN ENCLOSURE

In this chapter, we describe the theory for modes in a rectangular room and the distribution of adjacent eigenfrequency spacing. The distribution exhibits a non-zero value at zero spacing, which corresponds to the presence of degeneracies. In contrast, we discuss the distribution of frequency spacing of an irregular geometry in the shape of a stadium. For the stadium, small frequency spacings are less probable and large frequency spacings are improbable. The spectrum exhibits apparent mutual repulsion of eigenvalues near the mean.

A. RESONANT MODES IN A RECTANGULAR CAVITY

The resonant modes within a rectangular cavity of dimensions L_x , L_y , and L_z (length, width and height) can be predicted using the standing wave solutions of the wave equation. Substitution of

$$p(x, y, z, t) = X(x)Y(y)Z(z)e^{j\omega t}, \quad (2.1)$$

where $p(x, y, z, t)$ is the pressure, into the wave equation and separation of variables (X , Y , and Z) results in the set of equations,

$$((d^2/dx^2) + k_x^2)X = 0 \quad (2.2)$$

$$((d^2/dy^2) + k_y^2)Y = 0 \quad (2.3)$$

$$((d^2/dz^2) + k_z^2)Z = 0, \quad (2.4)$$

where k_x , k_y , and k_z are the components of the wave vector. The separation constants are related by

$$(\omega/c)^2 = k^2 = k_x^2 + k_y^2 + k_z^2, \quad (2.5)$$

where $\omega = 2\pi f$, the angular frequency in radians per second (rad/s) and c is the speed of sound in the medium (~343m/sec in air at room temperature).

Application of the boundary conditions

$$(\partial p / \partial x)_{x=0} = (\partial p / \partial x)_{x=L_x} = 0 \quad (2.6)$$

$$(\partial p / \partial y)_{y=0} = (\partial p / \partial y)_{y=L_y} = 0 \quad (2.7)$$

$$(\partial p / \partial z)_{z=0} = (\partial p / \partial z)_{z=L_z} = 0 \quad (2.8)$$

leads to the solution

$$p_{lmn} = A_{lmn} \cos \frac{l\pi x}{L_x} \cos \frac{m\pi y}{L_y} \cos \frac{n\pi z}{L_z} e^{i\omega_{lmn}t}, \quad (2.9)$$

where the components of wave vector k take on the values

$$k_x = l\pi/L_x \quad l = 0, 1, 2, \dots \quad (2.10)$$

$$k_y = m\pi/L_y \quad m = 0, 1, 2, \dots \quad (2.11)$$

$$k_z = n\pi/L_z \quad n = 0, 1, 2, \dots \quad (2.12)$$

Thus, the allowed frequencies are quantized according to,

$$\omega_{lmn} = c \sqrt{\left(\frac{l\pi}{L_x}\right)^2 + \left(\frac{m\pi}{L_y}\right)^2 + \left(\frac{n\pi}{L_z}\right)^2} \quad (2.13)$$

The form of Equation (2.9) gives three-dimensional standing waves in the cavity with nodal planes parallel to the walls. If the eigenfunctions in the rectangular cavity are decomposed into traveling plane waves, then the standing wave solution can be viewed as a superposition of traveling waves whose directions of propagation are fixed by the boundary conditions. It is the coherent combination of these waves, each traveling obliquely with respect to the coordinate axes, that results in the three-dimensional standing wave of Equation 2.9 (Kinsler, et al. 1982).

B. DISTRIBUTION OF FREQUENCY SPACINGS

Ray and wave acoustics provide a complete approach to understand the theory of the behavior of sound in an enclosure. The wave equation can be solved exactly for a simple enclosure such as the rectangle. In complicated enclosures, such as the stadium geometry, the wave equation cannot be solved analytically; however, wave theory has been used to supplement and extend results predicted by ray-acoustic methods (Kinsler, 1982). In some publications, the ray-acoustic theory is also called *billiards* where the motion of a ball is traced within the enclosure (Berry, 1981, Stöckmann and Stein, 1990).

In a simple enclosure such as the rectangle, the distribution of the eigenvalue frequency separation (Δf) between adjacent modes is one statistical measure of the spectrum. The spacing for the rectangle should have a histogram that peaks at small frequency separation (indicating clustering) and follows a Poisson distribution as the frequency spacings increase (Berry, 1987). Figure 2.1 is a histogram plot of the theoretical eigenfrequency separation for the rectangle used in this experimental thesis for frequencies up to 15KHz.

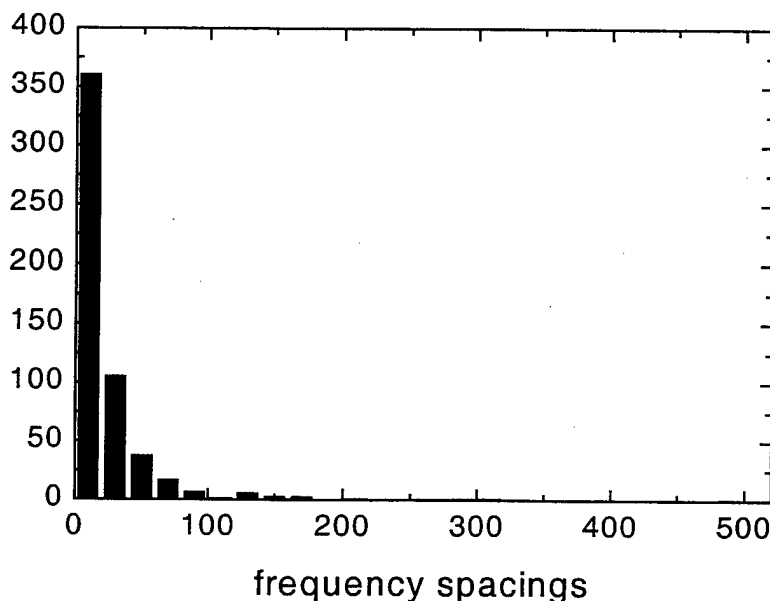


Figure 2.1 Theoretical distribution of spacings between neighboring eigenfrequencies up to 15 kHz for a rectangular room 21.5 cm long, 16.5 cm wide, and 3.22 cm high. The clustering of low frequency spacings corresponds to near degeneracies of modes of the room.

For a cavity with stadium geometry, the repulsion of frequency spacings is expected due to the general signature of ray chaos, despite the symmetric geometry of the stadium. Figure 2.2 shows a typical histogram distribution curve of energy level spacings for a stadium boundary. For the stadium, small spacings

are less probable and large spacings are improbable. The spectrum exhibits apparent mutual repulsion of eigenvalues near the mean (McDonald and Kaufman, 1987). For a given bin size of frequency spacing (Δf) the number of actual occurrences of frequency differences ($N(\Delta f)$) between two neighboring eigenfrequencies throughout the spectrum is plotted.

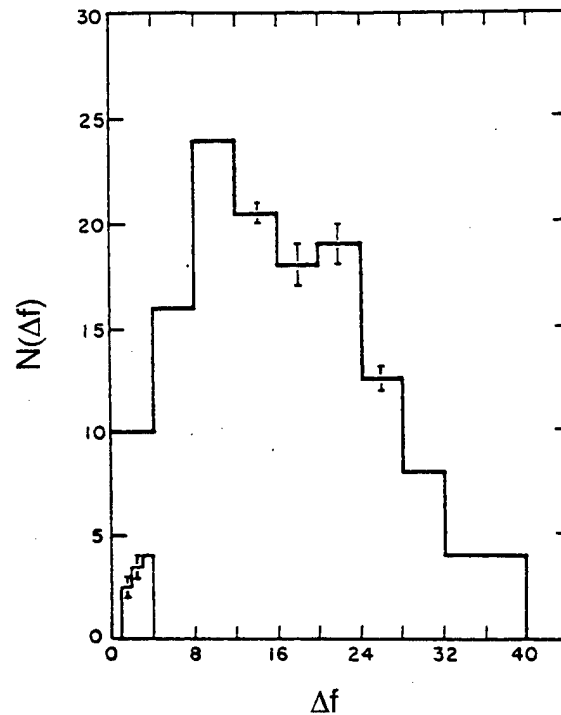


Figure 2.2. Theoretical distribution of spacings between neighboring eigenfrequencies in a two-dimensional stadium boundary (From McDonald and Kaufman, 1987). At low frequency spacings, there is no clustering, indicating level repulsion.

For frequency separation between two adjacent modes, clustering at low frequency spacings is not the predominant characteristic to be expected due to repulsion between the levels in the stadium. It has been shown that the eigenvalue spectrum and eigenfunctions of a linear operator whose (short-wave limit) rays are stochastic, exhibit, respectively, mutual repulsion of neighboring

eigenvalues and random directionality of nodal curves (McDonald and Kaufman, 1987). In other words, unlike for regular geometries, the eigenvalues for a stadium-shaped cavity are non-degenerate.

III. APPARATUS

The main components of the apparatus are the stadium-shaped acoustic cavity, a JBL 2450H compression driver, and a $\frac{1}{8}$ inch and a $\frac{1}{4}$ inch B&K microphones.

A. ACOUSTIC CAVITY

The acoustic cavity consists of plexiglass hollowed in a stadium shape and mounted on 3 plexiglass legs. The stadium dimensions are 38 cm long, 16.5 cm wide, and 3.22 cm high. The semicircles that give the stadium shape have a radius of 8.25 cm. Figure 3.1 is a diagram of the top view of the cavity.

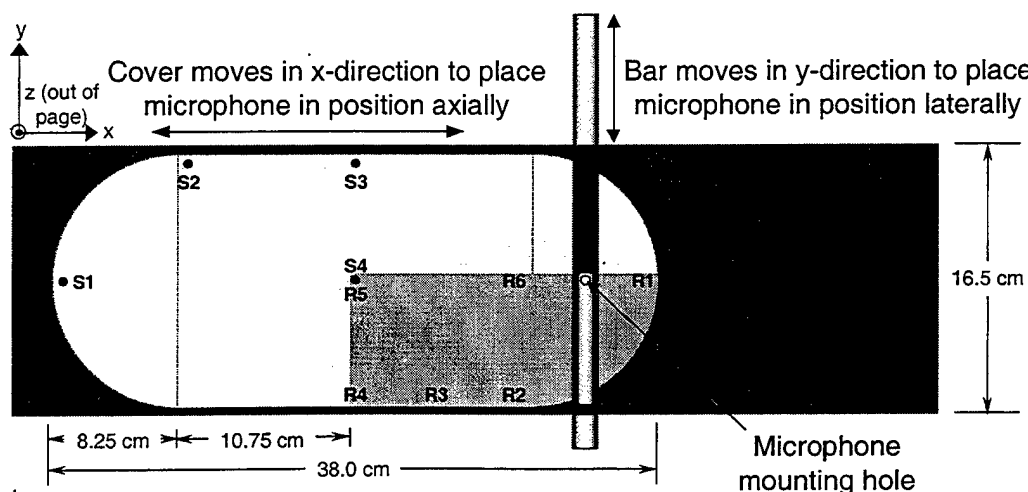


Figure 3.1. Top view of the basic resonator configuration. The cavity is made of plexiglass with inner dimensions 38 cm long, 16.5 cm wide, and 3.22 cm high. The semicircles that give the stadium shape have a radius of 8.25 cm. A sliding cover moves the microphone along the length of the cavity, while a sliding bar moves it along the width of the cavity. Modes of the room are excited at source locations S, and the acoustic response is measured at specific receiver locations R, or throughout the shaded region.

Two semi-circular plexiglass inserts of radius 8.25 cm and 3.22 cm in height were used to create a rectangular cavity of 21.5 cm length and 16.5 cm in width. Four holes (at source points S1 through S4 in Figure 3.1) of approximately 0.165 cm diameter were placed in the base of the cavity to allow the compression driver to be coupled to the cavity and excite modes.

The plexiglass cover of the cavity was sized to contain the entire cavity while allowing motion of the cover along the length (x-axis) of the stadium. The cover is fitted with a mobile arm which has a ¼ inch mounting hole for the microphone described below. This arm allows travel of the microphone along the width (y-axis) of the cavity. The cover and mobile arm enables any quadrant of the stadium to be monitored by a microphone. By moving the cover lengthwise and the arm across the width of the cavity, the frequency response of the room was measured at the receiver points R1 through R6, while mapping of the resonant modes was performed within the quadrant indicated by the shaded region in the figure. High vacuum grease was used to improve the acoustic seal between the cover and the cavity.

B. ACOUSTIC DRIVER

A JBL 2450H compression driver provided the desired acoustic signal into the cavity. The driver is rated from 500 Hz to 15 kHz. Two different sources were used to drive the unit for different sections of the experiment. The internal source of the Hewlett Packard 35670A Dynamic Signal Analyzer was used for plotting the resonant peaks across the 400 to 15,200 Hz swept sine wave

spectrum. This signal was sent to channel 1 (CH1) of the Signal Analyzer. An Hewlett Packard HP33120A 15MHz Function/Arbitrary Waveform Generator was used to drive the unit for mapping the mode structure for a single input frequency sine wave. The source signal from these devices was then sent through an Hewlett Packard 467A Power Amplifier and then onto the compression driver. The driver was coupled to the cavity by a 22.5 cm length of plastic tubing between the pipe in the cover of the driver and the source pipe at the base of the enclosure. This plastic tubing permitted the sound field to enter the cavity through mounting holes in the floor of the cavity.

C. MICROPHONE

Acoustic field measurements were made within the cavity at various points (Figure 3.1) using the mounting arm and stadium cavity cover assembly described above. The spectrum was measured using Brüel and Kjaer ¼ inch and ⅛ inch condenser microphones (Cartridge Type 4136). Measurements were taken at the ceiling of the cavity through a hole in the mobile sliding arm mount.

The microphone was mounted in the cover/arm assembly and powered by the Brüel and Kjaer Microphone Power Supply (Type 1801). The output signal was sent through an Ithaco 1201 Low Noise Pre-Amplifier. From the pre-amp, the output was sent to channel 2 of the Tektronix 2465 300MHz Oscilloscope and to channel 2 of the HP 35670A Signal Analyzer mentioned above.

For the stadium, the source was placed at position S1 (Figure 3.1), and the spectral frequency response was measured at locations R1 through R6. For

the rectangular box (stadium with inserts), the source was placed at S2 and the receiver at R2.

Nodal mapping in the stadium was conducted placing the source at point S1 and moving the cover/mounting arm assembly to traverse one quadrant of the stadium at the opposite end of the cavity (see Chapter IV). Symmetry in the geometries of the stadium and rectangle require only one quadrant of the cavity to be mapped.

IV. SPECTRAL AND MODE MEASUREMENTS OF THE CAVITIES

A. SPECTRUM MEASUREMENT

The resonant peaks for both the rectangular and stadium geometries were measured from 450 Hz to 15 kHz. The lower limit was chosen to be well below the theoretical frequency (797 Hz) for the expected first mode ($l, m, n, =1, 0, 0$) of the rectangular cavity. The upper limit was based on the maximum rating of the JBL acoustic driver.

Initially, a resolution of 1 point per Hz was set. This was performed by selecting a frequency bandwidth of 1600 Hz using a swept sine signal with the signal analyzer frequency resolution at 1601 points per sweep. Poor results were obtained using this resolution – namely, less than 80% of predicted modes below the frequency for the first vertical mode (0,0,1) were identified in the rectangle. With a smaller bandwidth of 800 Hz and a resolution of 1601 points/sweep (or 2 points/Hz), good agreement occurred up to frequencies below the first vertical mode, but began to degrade at frequencies above this value. Thus, the bandwidth was reduced to 400 Hz at frequencies above 5250 Hz. For example, the 5250 to 5650 Hz bandwidth was swept with a resolution of 1601pts/sweep, equaling 4 data points/Hz. This resolution/bandwidth combination was maintained until 15 kHz.

1. Rectangular Cavity

The rectangular cavity was formed using the semi-circular plexiglass inserts (described in Chapter III.A) placed at the two ends of the stadium. The acoustic driver was coupled to the cavity at source point S2, the corner of the rectangle. The microphone was located at receiver point R2, the corner located diagonally across the rectangle, and mounted flush in the sliding arm/cover assembly. For this configuration of source and receiver, all resonant modes can be excited and detected.

The amplified output of the HP35670A Dynamic Signal Analyzer internal source was used as the input into the JBL compression driver. The input signal has a $1V_{pk}$, linear swept sinusoidal waveform.

The signal from the microphone was passed through a pre-amplifier and filter for optimum display using the oscilloscope and channel 2 of the signal analyzer. The filter settings of the pre-amp were between 300 Hz and 30 kHz, with the gain set at 1000.

The spectrum data was then saved to disk using the 3½ inch internal drive of the signal analyzer. This data was then converted to ASC II format and read by Microcal™ Origin™ software version 5.0 and plotted. Figure 4.1 is a plot of the rectangular spectrum with the S2–R2 source-receiver combination.

The resonant modes of the rectangular geometry were then counted by visual inspection of the data and use of Origin™ to step through each data point in a given sweep to locate a mode. Modes included maximum peaks in the plotted curves and “shoulders,” or inflection points, where flatter areas of the

curve might indicate a mode.

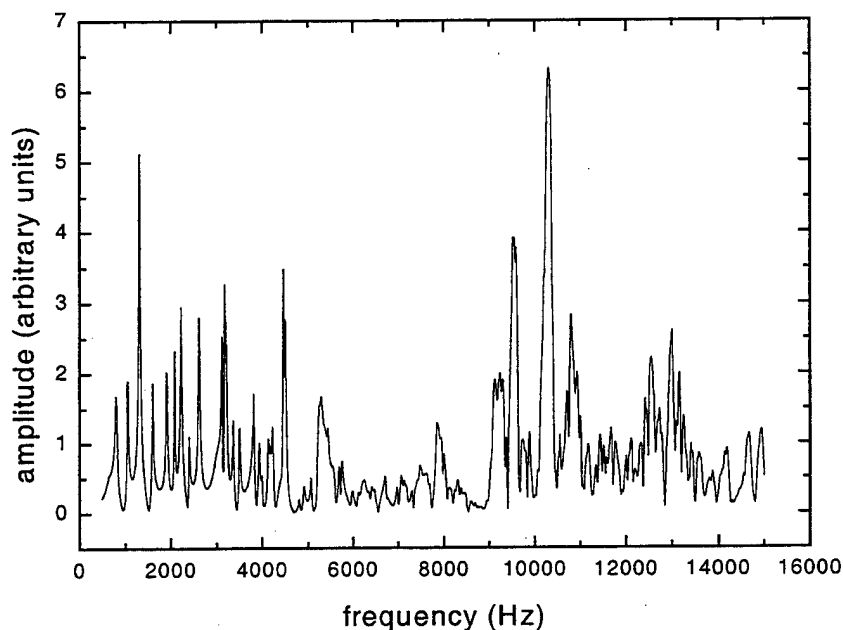


Figure 4.1. Frequency spectrum of modes in a rectangular cavity of dimensions 21.5 cm length, 16.5 cm width, and 3.22 cm height.

This information was compared to the theoretical data predicted for the rectangular geometry of the cavity actual dimensions. Table A.1 in the Appendix contains a listing of theoretical frequencies (f_{theor}) at or below the frequency for the first vertical mode ($f_{\text{co}} = 5,376$ Hz for mode (0, 0, 1)). The experimental frequency (f_{exp}) data is also presented for comparison and to calculate the frequency separation between modes. The frequency separation between adjacent modes are included for both the theoretical and experimental modes, Δf_{theor} and Δf_{exp} , respectively.

Experimentally, all 34 of the modes expected at, or below cutoff frequency were identified in the experimental data. The experimental values were

compared with the calculated values with an average of 0.19 percent error for modes with $f \leq f_{co}$. A total of 553 theoretical modes are expected to exist below 15 kHz. The ability to identify resonant peaks degraded above 7 kHz. Seventy-three of the seventy-seven expected modes (94.8 percent) were experimentally identified below 7 kHz. Between 7 and 9 kHz, only 71.6 percent are seen. These percentages dropped to 53.3% from 9 to 11 kHz, 31.0% from 11 to 13 kHz, and 21.1% for the band 13 to 15 kHz. Overall, 251 of 553 predicted modes (or 45.4%) were experimentally identified for the spectrum below 15 kHz.

2. Stadium Cavity

Resonant modes for the stadium geometry were measured by the same method described above from 450 Hz to 15 kHz. The plexiglass inserts used to form the rectangular geometry were removed from the cavity.

Initial measurements were conducted using the source-receiver combination S1-R1 (Figure 3.1). Figure 4.2 shows the resultant spectrum plot. A lower frequency initial mode is seen at 496 Hz.

Resonant modes were counted in the same manner as for the rectangle. Twenty-five modes were identified below the frequency of the first vertical mode, $f_{co} = 5,326$ Hz. This frequency is the same as for the rectangle, due to the same height dimension L_z .

Nine additional measurements were made using various source-receiver configurations to determine if different resonant modes would be excited using different source-receiver locations within the cavity. With the source at point S1, the microphone was placed at receiver points R2, R3, R4, and R5, and spectrum

plots were obtained separately. Separate measurements were also obtained using source point S2 and receiver points R1 through R5 (see Figure 3.1). These measurements failed to yield any new frequency modes. In general, the same resonant peaks were identified, however, with different amplitudes of the peaks, dependent upon the source and receiver locations.

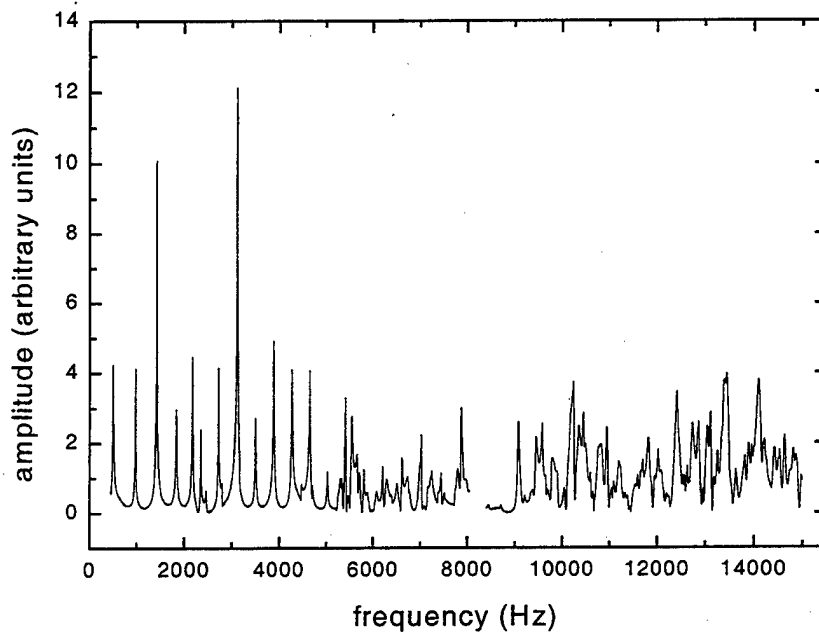


Figure 4.2 Frequency spectrum of modes in a stadium-shaped cavity of dimensions 38 cm length, 16.5 cm width, and 3.22 cm height. The semicircles that give the stadium shape have a radius of 8.25 cm.

B. FREQUENCY SPACING

Histograms of the separation between adjacent frequency modes, Δf , were determined from the theoretical predicted modes for the rectangular geometry and the experimental frequency mode data obtained from both the rectangular and stadium geometries.

In the rectangular geometry only experimental modes which were determined to be adjacent based on the predicted theoretical data were used for the frequency separation histogram plots. The data contained 155 pairs of frequencies adjacent to one another. Figure 2.1 is the theoretical histogram plot of frequency spacing for the rectangular cavity. Figure 4.3 is the experimental frequency spacing histogram for the rectangle.

All modes identified in the stadium up to 7 kHz were used to plot the frequency spacing histogram. This frequency was chosen to ensure the majority of modes identified in the stadium could be considered adjacent. The experiment in the rectangle showed the ability to predict modes above this frequency was unreliable when the data was compared to the theoretical values. This method assumes the data obtained in the stadium had similar reliability as that in the rectangle. The modes in the stadium tend to repel one another, vice cluster as in the rectangle. Therefore, in general, one should expect the frequency separations in the stadium to be larger, particularly at lower frequencies. Larger Δf values make the modes more likely able to be resolved by the analyzer. Figure 4.4 is the histogram plot for stadium data obtained experimentally.

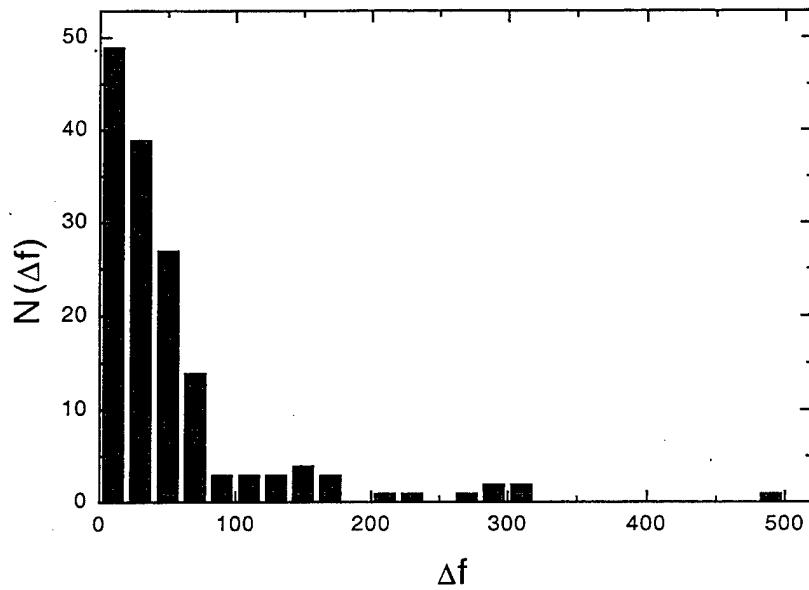


Figure 4.3. Experimental distribution of frequency spacings between neighboring eigenfrequencies up to 15 kHz for a rectangular room 21.5 cm long, 16.5 cm wide, and 3.22 cm high. The clustering of low frequency spacings corresponds to near degeneracies of modes of the room.

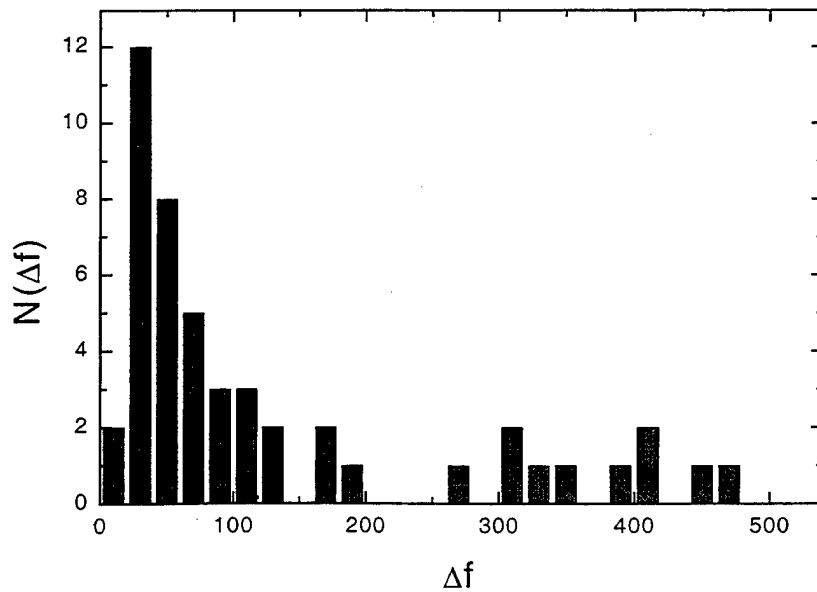


Figure 4.4. Experimental distribution of frequency spacings between neighboring eigenfrequencies up to 7 kHz for a stadium room 38 cm length, 16.5 cm width, and 3.22 cm height. The semicircles that give the stadium shape have a radius of 8.25 cm. At low frequency spacings, there is no clustering, indicating level repulsion.

C. NODAL MAPPING

1. Rectangular Cavity

The cavity cover/mounting arm assembly was used to move the microphone within one quadrant of the rectangular cavity. A measuring scale was affixed to the side of the enclosure to measure the lateral position (x-axis) of the microphone within the cavity. A similar scale was placed on the mounting arm to measure the microphone's position (y-axis) along the width of the chamber. The ¼ inch microphone was mounted in the arm flush with the ceiling of the cavity formed by the cover (approximately 3.2 cm above the floor of the cavity).

The cover/arm assembly was moved back and forth laterally (along the x-axis) with the microphone fixed along the width (y-axis). The quadrant was "swept" by conducting adjacent lateral swaths at 0.5 cm separation. Subsequent swaths would be conducted using the microphone at a position 0.5 cm from the previous sweep (y-position). This distance between swaths was chosen based on the resolution of the microphone (estimated to be ± 0.15 cm). The mapping was then confirmed by conducting a second sweep; however, with the arm moved along the width (y-axis), with the microphone x-position held fixed for the initial sweep. Subsequent sweeps were conducted after moving the cover 0.5 cm laterally (along the x-axis). This process was repeated until the entire quadrant was covered.

A resonant frequency was chosen and entered into the signal generator as a sinusoidal waveform. An amplitude of $0.6 V_{pp}$ was input to the driver and displayed on the Channel 1 of the oscilloscope.

The microphone was initially placed at the corner (R2, $x = 10.1$ cm, $y = 0.4$ cm) of the cavity located diagonally across the rectangle from the source (S2). These (x, y) points prevented the microphone from hitting vertical walls of the cavity during the motion of the microphone cover/arm assembly. The output of the microphone was displayed on the Channel 2 of the oscilloscope. The frequency was adjusted incrementally using the signal generator to produce a maximum amplitude response signal from the microphone. All filter settings for the pre-amp remained the same as in the Spectrum Measurement section, but the gain was adjusted to as low as 500 and to as much as 2,000 to produce a display which enabled phase shifts to be easily observed on the oscilloscope. Nodes could be seen in the display as the sinusoidal signal approached a minimum and shifted 180° phase while the microphone was moving.

The microphone was then positioned back to the point where the minimum was located, and the (x, y) coordinates of this position were recorded by hand. Resolution using this method is estimated to be approximately ± 0.15 cm based on the radius of the microphone. Figures 4.5 and 4.6 show the nodal plots of one the quadrant in the rectangular geometry for experimental frequencies 2,397 Hz (3, 0, 0) and 5,051 Hz (5, 3, 0). No reliable nodal mapping data could be obtained within the rectangular geometry above 7 kHz.

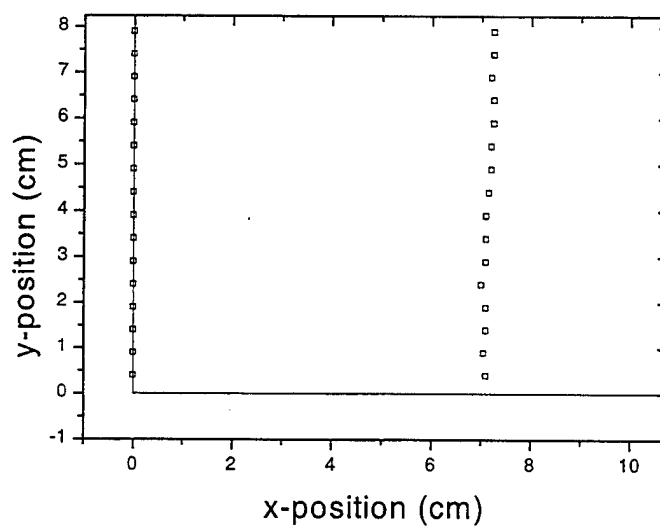


Figure 4.5. Pressure nodal lines for the (3,0,0) mode of one quadrant of the rectangular cavity. In a rectangular room 21.5 cm long, 16.5 cm wide, and 3.22 cm high, the resonant frequency of this mode is 2,397 Hz. The size of the data point corresponds roughly to the resolution of the microphone.

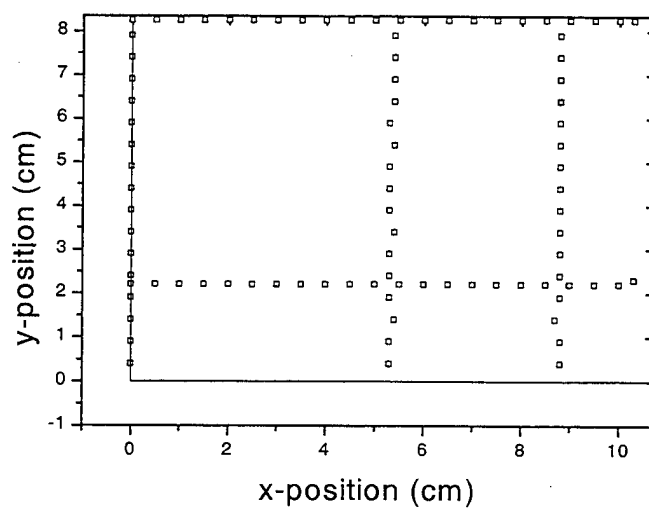


Figure 4.6. Pressure nodal lines for the (5,3,0) mode of one quadrant of the rectangular room. In a rectangular room 21.5 cm long, 16.5 cm wide, and 3.22 cm high, the resonant frequency of this mode is 5,051 Hz. The size of the data point corresponds roughly to the resolution of the microphone.

2. Stadium Geometry

The same method described in the previous section was used to conduct mapping within the stadium. With the source at location S1, Figures 4.7 and 4.8 are the plots of the pressure nodal lines for the experimental frequencies 2,723 and 7,436 Hz, respectively. No reliable nodal maps were obtained in the stadium at frequencies above 8 kHz. Additional frequencies were mapped to determine if a pattern evolved as the resonant frequencies were increased.

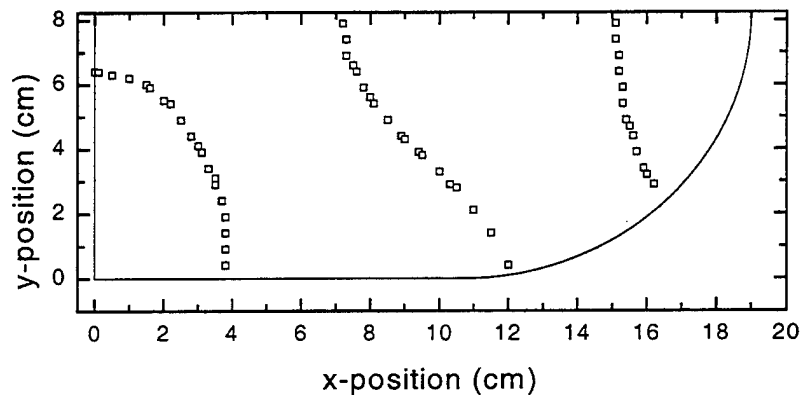


Figure 4.7. Pressure nodal lines of one quadrant of the stadium cavity. The resonant frequency of this mode is 2,723 Hz. The size of the data point corresponds roughly to the resolution of the microphone.

Apparent from Figures 4.7 and 4.8 is the fact that an analytical solution for modes of a stadium cannot be obtained. The nodal curves are seen to be irregular in direction and their separation is roughly regular representing the half wavelength $c/2f$. There are no nodal crossings in the interior. In the high frequency limit, this system is particularly simple because the ray trajectories are stochastic for all nonzero values of the aspect ratio $\gamma = L/R$ between the length L

of the straight side and the radius R of the semicircle. The degree of stochasticity increases from zero at $\gamma=0$ (the circle) to a flat maximum near $\gamma=1$ (Benettin and Strelcyn, 1978).

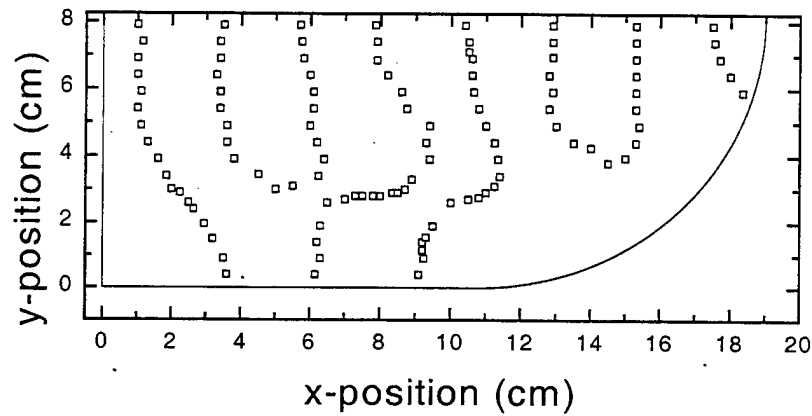


Figure 4.8. Pressure nodal lines of one quadrant of the stadium cavity. The resonant frequency of this mode is 7,436 Hz. The size of the data point corresponds roughly to the resolution of the microphone.

V. TIME-REVERSAL ACOUSTICS

A. OVERVIEW

Over the past few years, a resurgence of interest in the phenomenon of time-reversal acoustics (TRA) has occurred. The increase in hardware and computational complexity has allowed a more thorough and general study of this feature of acoustic propagation beyond the earlier, somewhat crude trials in the mid-1960's. Recent experimental work in the Mediterranean by Kuperman et al. (1998) has shown that the focusing properties of a time-reversed signal can be quite good, and under some circumstances may be stable for extended periods of time. Their work showed a stable focus at 445 Hz could be maintained for more than a week. Additional experimental data will be reported soon by the same group in the same location at a higher frequency of 3.5 kHz.

Time-reversal acoustics (TRA) is fundamentally based on the principle of reciprocity. For example, a single point-like source will excite numerous propagating modes in a shallow water waveguide. Due to differences in the mode group speeds, these modes will disperse and arrive at a distant receiver as multipath structures. A full water column array of receivers/sources can record the arrival structure of the modes. By time reversing the signal received at each element and then synchronously re-transmitting these time-reversed signals, the received modes are transmitted outward from the array in the opposite order from which they arrived. Because the path back from the array to the original

source location is reciprocally identical (barring significant currents or other features that degrade reciprocity), the mode group speeds are also identical. Therefore, all of the modes arrive back at the original source location at the same time and add up constructively. This generates both a temporal and spatial (range and depth) focusing of the propagating field.

Because the focus resolution is based in large part on the number of different propagating modes, or multipaths, which are resolved in the received signal, the quality of the focus does not degrade significantly with range. On the contrary, larger propagation ranges may improve the temporal focus footprint since increases in multipaths enhance the peak to sidelobe levels, although a natural limit to this certainly exists. In addition, since a time-reversed signal allows a TRA system to pump more energy into the water (spread over the multipaths), more energy is available for reception at the focus location than would have been from a simple, coherent source transmission (a "ping"). The focusing of the multipaths then further enhances the received signal amplitude, improving the signal-to-noise ratio at the focus location.

Similarly, the TRA technique can also be used to reduce the appearance of reverberation in a room. Surprisingly, in this case not an array of elements, but a single element is required and a one-point time-reversal in a cavity produces better results than a wide aperture time-reversal array in an open system. Using reflections at the boundaries, focusing quality is not aperture-limited because the collapsing wave front approaches the focal region from all directions. As in the case of a shallow water waveguide, the focus resolution is

based in large part on the number of the different multipaths.

1. Signal Processing Technique

Figure 5.1 illustrates the TRA process. The initial signal (Figure 5.1a) in this case is an 8 kHz, two-cycle pulse with a Hanning window source spectra and a peak amplitude of 5 Volts AC. It was generated by the arbitrary function generator of a Gage 8-channel data acquisition system operating at 5 MHz and sample depth of 50,000 samples. The signal is transmitted from location S1 (see Figure 3.1) using a JBL 2450H compression driver.

A 1/4" B&K microphone located at R6 (see Figure 3.1) recorded the initial reception (Figure 5.1b), and stored it in memory of the digital scope of the Gage data acquisition system. Using a Matlab software algorithm developed by Michael Heinemann (1999), the initial reception was reversed in time (Figure 5.1c) and re-transmitted into the enclosure from the original location S1 by the JBL 2450H compression driver. Thus, the last arrival is retransmitted first and first arrival is retransmitted last.

With the microphone still at location R6, a second reception is recorded (Figure 5.1d), showing focusing in time. Note that the retransmission is omnidirectional and that the information about the direction of each measured front is lost. Due to reciprocity, as long as the original source/receiver points are the only ones used in the operation, the time-reverse transmission and subsequent reception can be performed, undistinguishable by either point. In fact, in each of the analyses that follow, the source and receiver remained in their original positions during the time-reversal transmission. At other points within the

enclosure, the different paths do not add coherently, and no focusing occurs.

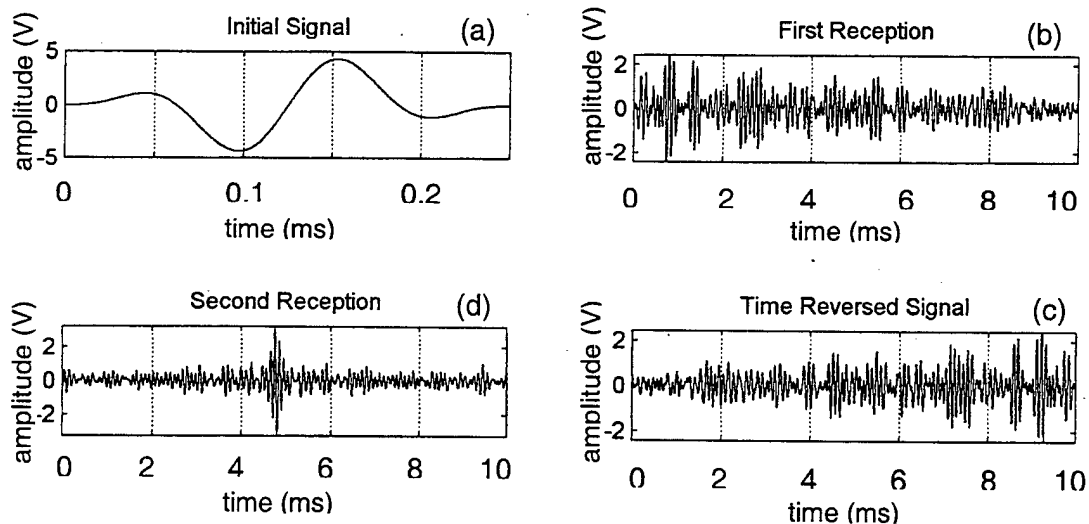


Figure 5.1. Example of the time-reversal acoustics technique. (a) A two cycle, 8 kHz, pulse in a Hanning window is generated at some point in the enclosure. After several reflections the wave field distributes in the room. (b) The resulting wave field is recorded by a microphone at a different location during a time $T=10$ ms. (c) The recorded signal is time-reversed and retransmitted by the original source, yielding the time record (d) at the microphone, with an observed SNR of approximately 2.9.

2. Sound Propagation

To illustrate the basic principle of the TRA technique, consider the schematic rendition of sound propagation in one half of the stadium. A short pulse of finite duration is emitted from a point in the enclosure. The sound waves emanate from the source, spreading in a spherical manner until the boundaries are encountered, as shown in Figure 5.2a. After several reflections (Figures 5.2b, 5.2c) the sound field acquires a foggy distribution in which the wave fronts can no longer be distinguished (Figures 5.2d, 5.2e).

At another point, the resulting wave field is recorded during a long period of time. After time reversing, the measured signal is retransmitted from the position of the microphone. The wave field passes again by a foggy distribution

(Figure 5.2e), until shortly before refocusing, a wave front emerges from the reverberant noise (Fig 5.2 f, 5.20g). The refocused signal has the same shape as the one that was initially emitted, but propagates in the reverse direction.

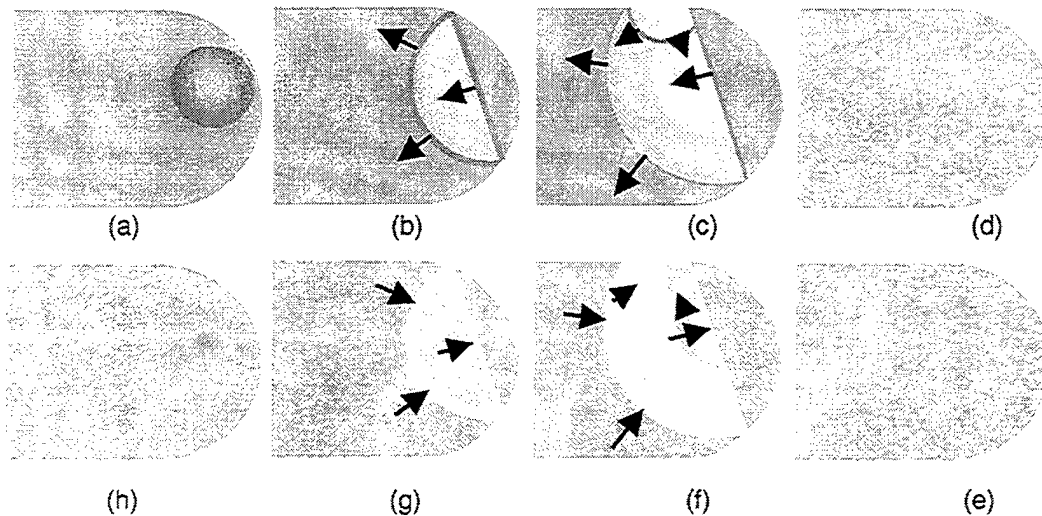


Figure 5.2. Schematic rendition of sound propagation a stadium-shaped room. (a)-(d) Sound of a short pulse is injected at a point in the room and after several reflections the wave field distributes in the room. (e)-(h) After emission of the time-reversed signal from the recording point, the signal refocuses.

If the positions of the source and receiver were not swapped as they were in the previous example, the propagation of the sound field would be very similar to that described in Figure 5.2. This is due to the reciprocity that exists between the source and the receiver. As we found in the analyses that follow, the only difference between swapping the transducers and having them remain in their original positions was that the focusing occurred at the source when the transducers were swapped, and at receiver when they remained fixed.

B. ANALYSIS

In order to determine the extent with which TRA can be utilized for de-reverberation in acoustic rooms for communications purposes, several analyses were performed. First, because the performance of this technique is dependent upon frequency, the performance of TRA as a function of frequency was evaluated. Next, because the signal to noise ratio depends on the size of the time record of the measured signal (Draeger and Fink, 1997), the time reversal window, various data window sizes were examined. Another important factor governing the application of TRA to encrypted communications is the size of the focal region of the resultant signal, so this was also explored. Using the semicircular wedges, we compared the focusing quality as a function of frequency, time reversal window size, and spatial extent for the rectangular and the stadium cavities. This comparison was consistently done with the source at S4, the center of the enclosure, and the receiver at R4 (see Fig 3.1). Finally, we also tested a multi-frequency scheme (Abrantes et al. 1999; Abrantes, 1999) where a single pulse of multiple frequencies was transmitted and its time-frequency spectrogram was evaluated.

1. TRA Focusing Quality as a Function of Frequency

The results of this analysis are shown in Figure 5.3. In the stadium enclosure, the signal to noise ratio (SNR, ratio of peak signal voltage level to peak reverberation or “noise” voltage level) is shown to be stronger than the SNR measured in the rectangular enclosure. The improved performance with

frequency up to frequencies near 14 kHz in the stadium enclosure may be due to the increasing number of multipaths as a function of frequency. On the other hand, the degradation of the signal for frequencies larger than 14 kHz, may be due to increasing attenuation as a function of frequency, or the driver rolling off. The overall poor performance in the rectangular enclosure may be due to the regular orbits of the acoustic rays and the subsequent lack of ergodicity of the distribution of sound intensity in the room.

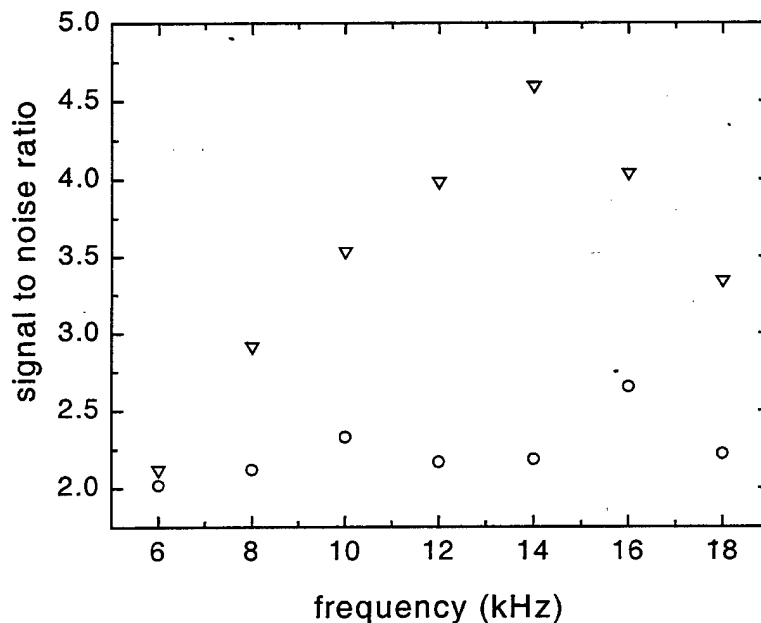


Figure 5.3. Focusing quality for various center frequencies of a two-cycle pulse. Plotted is the signal to noise ratio, SNR, as a function of frequency. The down triangles correspond to the SNR for the stadium enclosure, the open circles correspond to the SNR for the rectangle.

2. TRA Focusing Quality as a Function of Window Size

The initial reception was processed with a sampling rate of 5 MHz and a sample depth of 50,000 samples. The selection of the 5 MHz sampling rate was due to two considerations: it was a fast enough rate to provide excellent

resolution, yet it was slow enough to permit the processor to perform its functions reasonably quickly. Similarly, the decision to use 50,000 samples was not an arbitrary one. After attempting to use various sample sizes (from 20,000 to 120,000), 50,000 samples proved to yield the optimum signal to noise ratio. We attribute this to the fact that, for these particular enclosures (with a frequency band of 6 to 18 kHz and a sampling rate of 5 MHz), a window size less than 50,000 samples did not provide enough multipath reflections, and a window size greater than this introduced significantly more dissipation and background "noise."

The whole time record consists of "lower" modes, with fewer reflections and a more direct path between the source and receiver, and "higher" modes, where the number of reflections is higher. Thus, the focusing quality of TRA for different time window sizes can be a measure of the degree of degradation of the information contained in the reverberant signal. To this end, we determined the SNR when the time-reverse of the original signal was retransmitted at both "ends" of the data window.

a. Higher Modes

Depicted in Figure 5.4 is the time-reversed signal of the original measured record. The shaded region in the figure corresponds to the sample region that was subsequently retransmitted. As the window size decreases, the signal to noise ratio degrades. Below 30,000 samples, mainly the high modes containing very little information are sampled, and a poor SNR is expected because of high mode degradation.

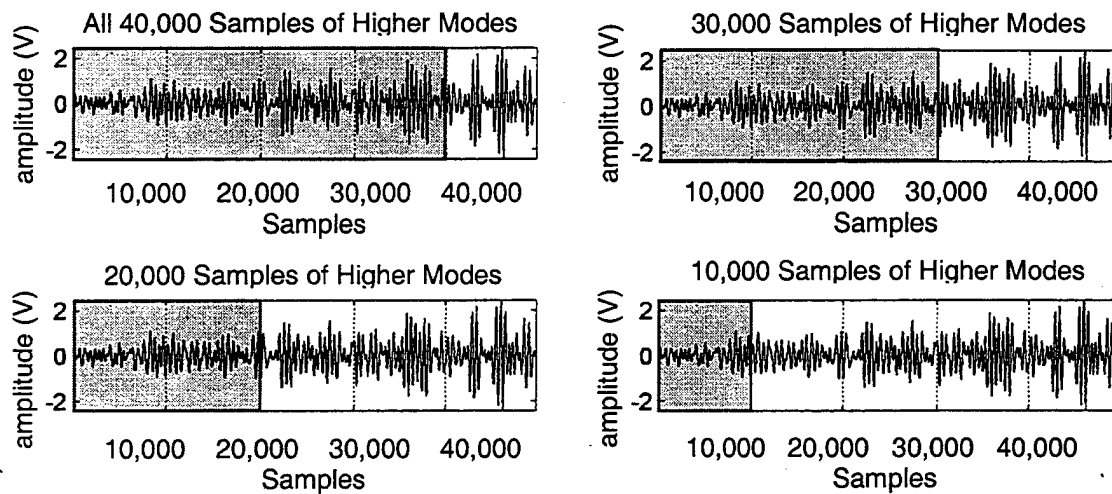


Figure 5.4. Time-reversed measured signal from a 14 kHz, two cycle initial pulse. The shaded region corresponds to size of the window used to determine the performance of the TRA as a function of window size. As the window size is reduced the signal to noise ratio degrades mainly because the high modes, containing very little information, are sampled.

b. Lower Modes

The lower mode data windows are depicted in Figure 5.5. As before, the shaded region in the figure corresponds to the sample region that was subsequently retransmitted. As expected, the signal to noise ratios continue to degrade, but in this case there is a fairly significant amount of information in the lower modes. This is because the lower modes contain more coherent energy than the higher modes. Consequently, as the window size is reduced the signal degradation is less when lower modes are included than when the higher modes are included. The conclusion of this analysis is that the lower modes appear to contain enough data to communicate effectively. Figure 5.6 illustrates the comparison between the higher and lower mode data window sizes.

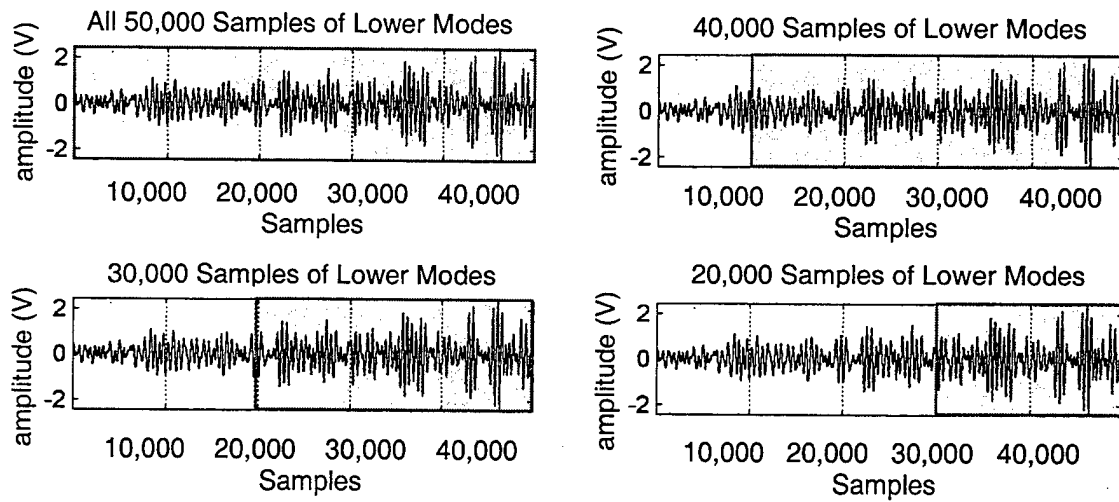


Figure 5.5. Time-reversed measured signal from a 14 kHz, two cycle initial pulse. The shaded region corresponds to size of the window used to determine the performance of the TRA as a function of window size. As the window size is reduced the signal to noise ratio degrades mainly because the multipath information is reduced.

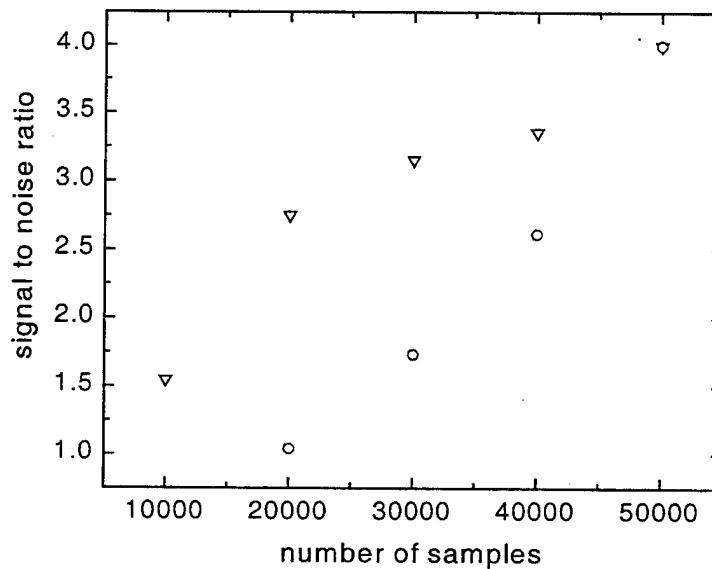


Figure 5.6. Focusing quality for varying time-reversal window sizes. The down triangles represent the lower modes, while the circles depict the higher modes. Because the lower modes contain more coherent energy than the higher modes, the signal degradation is less as the window size is reduced.

3. Extent of Spatial Focusing

We measured the spatial distribution of the re-focussed peaks of a 14 kHz, two-cycle pulse using the S4-R4 (Figure 3.1) source-receiver configuration. The cover of the chamber slides lengthwise on the rooms and the metal slide moves widthwise to position the $\frac{1}{8}$ inch microphone in both directions.

a. Focal Length

The length of the focal region was determined by sliding the top cover of the enclosure lengthwise in 0.5 mm increments, with the microphone positioned near the sidewall, and re-transmitting the time-reverse of the original measured signal at each increment. The same process was repeated with the wedges in place for the rectangular chamber. The results of this analysis are depicted in Figure 5.7. As shown in the figure, the focal length extends over less than one-half of a wavelength of 14 kHz for both the stadium-shaped and the rectangular-shaped rooms.

b. Focal Width

The width of the focal region was determined by sliding the metal bar widthwise in 0.5 mm increments toward the center of the enclosures. The results of these measurements are plotted in Figure 5.8. As shown in the figure, the widthwise SNR decreases more rapidly as a function of distance than the lengthwise SNR. Thus the focal spot does not exhibit circular symmetry. This asymmetry may be because the lengthwise measurements were done along the side walls of each of the rooms where there is a reinforcement of sound.

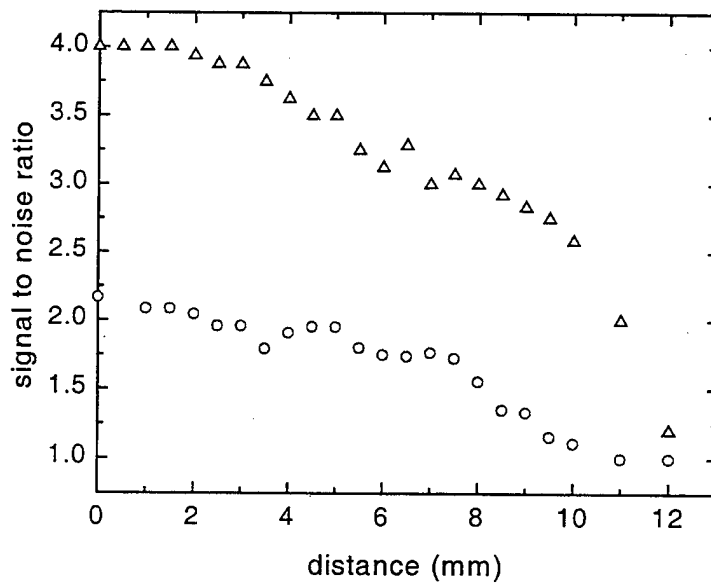


Figure 5.7. Lengthwise focal extent of a 14 kHz, two cycle pulse. The up-triangles correspond to the SNR as a function of lengthwise distance for the stadium-shaped room and the circles correspond to the SNR as a function of lengthwise distance for the rectangular shaped room. Note that the focal length extends over less than one-half of a wavelength of 14 kHz for both geometries.

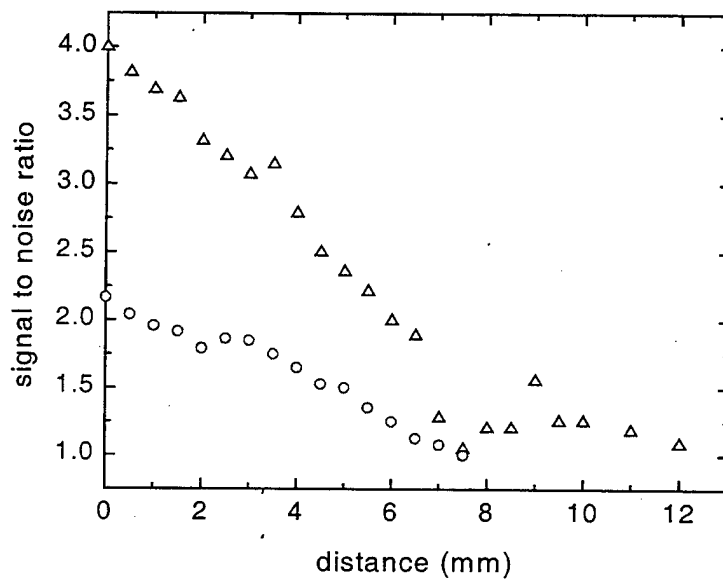


Figure 5.8. Widthwise focal extent of a 14 kHz, two cycle pulse. The up-triangles correspond to the SNR as a function of widthwise distances for the stadium-shaped room and the circles correspond to the SNR as a function of widthwise distance for the rectangular shaped room. Note that the focal width extends over less than one-half of a wavelength of 14 kHz for both geometries.

4. A Non-coherent Communication Scheme

The properties of time-reversal acoustics studied above suggest a potential application in the field of non-coherent acoustic communications. "Non-coherent" in this sense is meant to imply that no phase information will be transmitted in the communication signal but instead an energy detector method will be used. A novel communications scheme has been suggested by Abrantes et al. (1999) and Abrantes (1999) which employs both the temporal and spatial focusing properties of TRA. In this scheme, two source/receiver systems, **A** and **B**, are used to communicate with one another. A set of distinct signals representing binary bits is agreed upon and known by the **A** and **B** systems, both of which can filter and search for these specific signals in the presence of noise. Each signal should have roughly the same temporal resolution. A simple example would be multiple broadband signals with identical bandwidth, Hanning window source spectra, and center frequencies separated by half the bandwidth (allowing for null detection between adjacent signals). The total number of signals within the set is then limited primarily by the bandwidth of the system. For this example, let us assume there are four distinct signals (bits) within the set defining a 4-bit character (giving values from 0-15). The communications link is achieved when a single element of **A** transmits each signal to **B** with sufficient time between transmissions for all multipath structure to arrive. This provides **B** with the transfer function of the environment for those signals. Then **B** has the ability to transmit binary information to **A** by building 4-bit "symbols" out of the time-reversed signals. In addition, the transmission of subsequent symbols can

overlap each other significantly. The criterion for the delay between subsequent symbol transmissions is the temporal resolution of the focus. For example, if the signals originally transmitted by **A** have a nominal temporal resolution of 10 msec, then **B** is able to transmit the 4-bit symbols at a nominal rate of 100 symbols/sec. Furthermore, recall that these focused signals arriving back at **A** have an improved SNR. Now consider that multiple elements in **A** each uniquely transmit the communication signals. Depending upon the spatial focusing properties of the time-reversed signals, multiple symbols may be transmitted from **B** to focus at different locations along **A**.

In this section we report the first experimental realization of a TRA signal composed of two center frequencies, 12.5 kHz and 16.3 kHz, with an identical bandwidth of 3 kHz, and Hanning window source spectra. The source–receiver configuration is at S1–R6 (Figure 3.1)

Figure 5.9a corresponds to the initial pulse. The time record at the microphone of the first reception and the time-reverse signal are shown in Figures 5.9b and 5.9c, respectively. The second reception (Figure 5.9d) shows that focusing occurs. Figure 5.10 shows a spectrogram of the time record of the second reception (Figure 5.9d). The spectrogram evaluates the energy in the frequency bands as a function of time over a specific time window (0.5 ms). Thus a binary message can be determined this way. The time of arrival of the focus of the pulse is at 6 ms, as also indicated by Figure 5.9d.

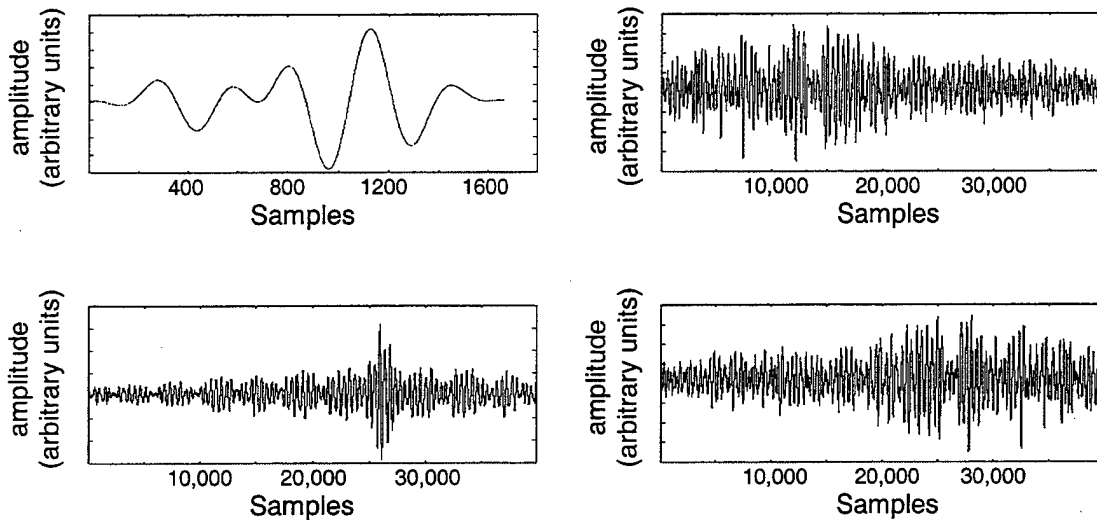


Figure 5.9. TRA sequence for non-coherent communications scheme. (a) The initial signal is a pulse with two center frequencies, 12.5 kHz and 16.3 kHz, with an identical bandwidth of 3 kHz, and Hanning window source spectra. (b) Time record of the transmitted pulse at the microphone. (c) The time-reversed measured signal. (d) The second reception shows that even with multiple frequencies, TRA process can focus to the intended target.

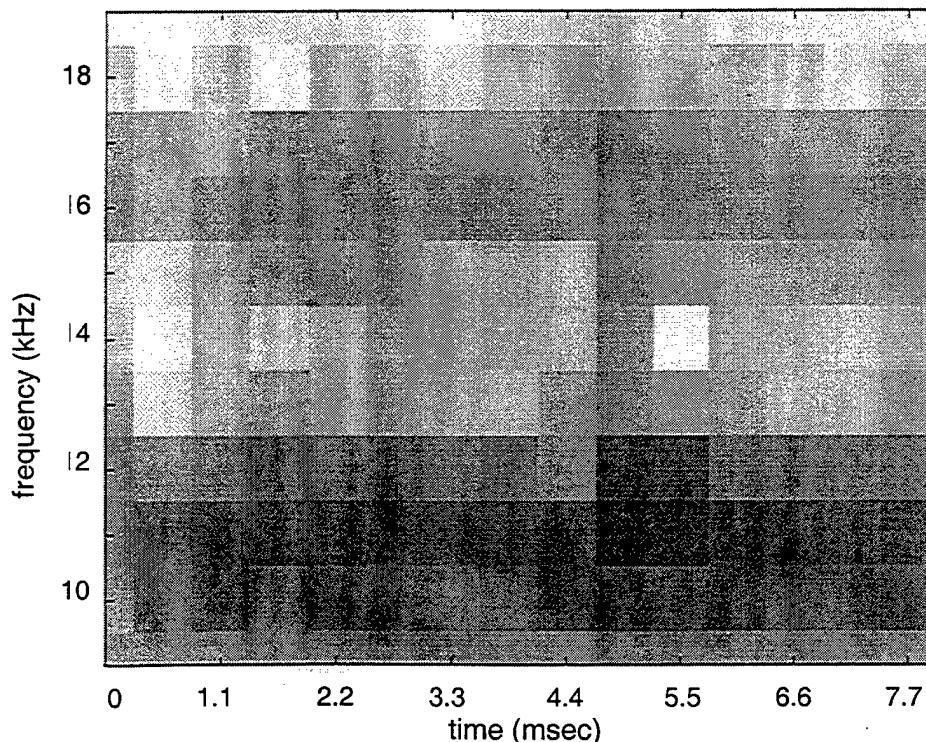


Figure 5.10. Received frequency spectrogram. The two frequency bands around 12.5 kHz and 16.3 kHz are highlighted, and focusing is shown to occur at about 5.1 msec. The darker shades represent the detection of the desired frequency bands; the lighter shades represent noise.

THIS PAGE INTENTIONALLY LEFT BLANK

VI. CONCLUSIONS AND FUTURE WORK

A. CONCLUSIONS

We have experimentally shown that the frequency spectrum and the shape of the modes for a regular geometry (the rectangular room) and an irregular one (the stadium-shaped room) exhibit drastically different characteristics. In regular geometries, clustering occurs for the smallest of frequency spacings, and the nodal curves are regular in direction and can cross. In irregular geometries, there are no nodal crossings in the interior, and mutual repulsion of neighboring eigenfrequencies and random directionality of nodal curves occur. In the short-wave-limit, these differences are related to rays that exhibit periodic orbit behavior for the rectangular room, and stochastic behavior for the stadium room.

We have also shown that time reversal in these two geometries yields results with large contrasts. In both geometries, we used a single time-reversal channel, which yielded better results than a wide aperture time-reversal array in an open system. Our measurements showed that for the stadium geometry, the focusing quality as a function of center frequency, time reversal window size, and spatial extent, was superior to the focusing quality for the rectangular geometry by about a factor of two. Surprisingly, the overall poor performance in the rectangular enclosure may be due to the lack of ergodicity of the distribution of sound intensity in the room. An equivalent time reversal experiment with billiards would yield opposite results because of strong sensitivity to initial conditions in

the stadium geometry.

We have been able to produce a clear acoustic message transmitted from one point of the room to the another. The spatial extent of the focus is a half wavelength of sound, indicating that the TRA possesses natural encryption for points other than the intended target. The focusing SNR of a time-reverse transmission can be improved by amplification and by using a larger window size (Draeger and Fink, 1997). On the other hand, residual temporal side lobes will persist due to multiple reflections, even for large window sizes. However, we found an optimal window size beyond which the SNR substantially degraded. The signal degradation may be due to higher modes that undergo large number of reflections and accumulate a mismatched phase due to dissipation, adding noise to the process.

We have also performed the first experimental realization of Abrantes et al (1999) communication scheme. The benefit of improving the SNR dramatically, coupled with the capability to communicate makes the TRA technique a very powerful and desirable method of communication.

B. FUTURE WORK

This research would benefit from further study. First, simultaneous communications of different messages to multiple locations within the cavity would test the power of this technique in a more rigorous, realistic communication scheme. Next, the performance of TRA for different locations in the room of source/receiver pairs could be explored. Another would be to

examine how relative motion affects the process by, say, moving the microphone during TRA.

THIS PAGE INTENTIONALLY LEFT BLANK

APPENDIX. SPECTRAL AND MODE MEASUREMENT DATA

l	M	n	f_{theor}	Δf_{theor}	f_{expt}	% error	Δf_{exp}
1	0	0	797.6744	241.7195	801	0.42%	236
0	1	0	1039.394	270.8061	1037	0.23%	274
1	1	0	1310.2	285.1488	1311	0.06%	288.5
2	0	0	1595.349	308.7199	1599.5	0.26%	309
2	1	0	1904.069	174.7192	1908.5	0.23%	169
0	2	0	2078.788	147.7888	2077.5	0.06%	148
1	2	0	2226.577	166.4466	2225.5	0.05%	176.5
3	0	0	2393.023	215.9804	2402	0.38%	213
3	1	0	2609.004	11.3965	2615	0.23%	7.5
2	2	0	2620.4	497.7817	2622.5	0.08%	494
0	3	0	3118.182	51.6635	3116.5	0.05%	59.5
3	2	0	3169.845	20.85236	3176	0.19%	20
4	0	0	3190.698	27.89555	3196	0.17%	19.5
1	3	0	3218.593	137.1319	3215.5	0.10%	147.5
4	1	0	3355.725	146.8733	3363	0.22%	140
2	3	0	3502.598	305.539	3503	0.01%	310
4	2	0	3808.137	122.4628	3813	0.13%	119
3	3	0	3930.6	57.77186	3932	0.04%	65
5	0	0	3988.372	133.2115	3997	0.22%	132.5
5	1	0	4121.584	35.99212	4129.5	0.19%	25.5
0	4	0	4157.576	75.82957	4155	0.06%	71.5
1	4	0	4233.405	219.7479	4226.5	0.16%	164
2	4	0	4453.153	8.192878	4390.5	1.41%	68
4	3	0	4461.346	36.2611	4458.5	0.06%	46.5
5	2	0	4497.607	288.4393	4505	0.16%	287.5
6	0	0	4786.047	11.03557	4792.5	0.13%	0.5
3	4	0	4797.082	100.5276	4793	0.09%	121
6	1	0	4897.61	165.0151	4914	0.33%	152.5
5	3	0	5062.625	134.3449	5066.5	0.08%	120.5
0	5	0	5196.97	21.03761	5187	0.19%	26
6	2	0	5218.007	22.793	5213	0.10%	18.5
4	4	0	5240.8	17.0299	5231.5	0.18%	21.25
1	5	0	5257.83	68.25675	5252.75	0.10%	73.25

Table A.1. Partial listing of theoretical frequencies (f_{theor}) at or below the frequency for the first vertical mode (0, 0, 1) of a rectangular room 21.5 cm long, 16.5 cm wide, and 3.22 cm high. The experimental frequency (f_{exp}) data is also presented for comparison and to calculate the frequency separation between modes. The frequency separation between adjacent modes are included for both the theoretical and experimental modes, Δf_{theor} and Δf_{exp} , respectively.

THIS PAGE INTENTIONALLY LEFT BLANK

LIST OF REFERENCES

- Abrantes, A.A.M., Smith, K.B., and Larraza, A. (1999). "Examination of time-reversal acoustics and applications to underwater communications," *J. Acoust. Soc. Am.*, **105**, p. 1364.
- Abrantes, A.A.M. (1999). "Examination Of Time-reversal Acoustics In Shallow Water And Applications To Underwater Communications," Master's Thesis, Naval Postgraduate School, Monterey, CA.
- Benettin, G., and Strelcyn, J.-M. (1978). "Numerical Experiments on the Free Motion of a point mass in a plane convex region: Stochastic Transition and Entropy," *Physical Review A*, **17**, pp. 773-785.
- Berry, M. V. (1981). "Regularity and Chaos in Classical Mechanics, Illustrated by Three Deformations of a Circular 'Billiard,'" *Eur. J. Phys.*, **2**, pp. 91-102.
- Berry, M. (1987). "Quantum Physics on the edge of Chaos," *New Scientist*, 19 November 1987, pp 44-47.
- Draeger, C. and Fink, M. (1997). "One-channel time reversal of elastic waves in a chaotic 2D-silicon cavity," *Phys. Rev. Lett.* **79**, pp. 407-410.
- Heinemann, M. G. (1999). "AARLCOM Matlab software to drive the Gage Data Acquisition System." *Unpublished*.
- Kinsler, L. E., Frey, A. R., Coppens, A. B., Sanders, J. V. (1982). *Fundamentals of Acoustics*, John Wiley and Sons, Inc., pp. 214-216.
- Kuperman, W.A., Hodgkiss, W.S., Song, H.C., Akal, T., Ferla, C., and Jackson, D.R. (1998). "Phase conjugation in the ocean: Experimental demonstration of an acoustic time-reversal mirror," *J. Acoust. Soc. Am.*, **103**, pp. 25-40.
- McDonald, S. W., and Kaufman, A. N. (1979). "Spectrum and Eigenfunctions for a Hamiltonian with Stochastic Trajectories," *Physical Review Letters*, **42**, pp.1189-1191.
- Stöckmann, H.-J., and Stein, J. (1990). "'Quantum' Chaos in Billiards Studied by Microwave Absorption," *Physical Review Letters*, **64**, pp. 2215-2218.

THIS PAGE INTENTIONALLY LEFT BLANK

INITIAL DISTRIBUTION LIST

1. Defense Technical Information Center.....2
8725 John J. Kingman Road, STE 0944
Ft. Belvoir, VA 22060-6218

2. Dudley Knox Library.....2
Naval Postgraduate School
411 Dyer Road
Monterey, CA 93943-5101

3. Engineering & Technology Curricular Office, Code 34.....1
Naval Postgraduate School
411 Dyer Road
Monterey, CA 93943

4. Prof. William Maier, Code PH/Mw.....1
Department of Physics
Naval Postgraduate School
Monterey, CA 93943-5002

5. Mr. William Glenney.....1
Deputy Director
CNO Strategic Studies Group
686 Cushing Road
Newport, RI 02841-1207

6. Prof. Andrés Larraza, Code PH/La.....3
Department of Physics
Naval Postgraduate School
Monterey, CA 93943-5002

7. Prof. Bruce Denardo, Code PH/Db.....1
Department of Physics
Naval Postgraduate School
Monterey, CA 93943-5002

8. Prof. Tom Hofler, Code PH/Hf.....1
Department of Physics
Naval Postgraduate School
Monterey, CA 93943-5002

9. LT David Liddy.....4
Dahlgren Division
Naval Surface Warfare Center
17320 Dahlgren Road
Dahlgren, VA 22448-5100
10. LCDR John Holmes.....1
Executive Officer
NCTS GUAM
PSC 488 Box 100
FPO AP 96537